Reprinted from

PHYSICA D

Physica D 123 (1998) 437–447

Frequency analysis of discrete breather modes using a continuous wavelet transform

Kyle Forinash *, W. Christopher Lang

Natural Sciences Division, Indiana University Southeast, New Albany, IN 47150, USA

ELSEVIER


ELSEVIER

Physica D 123 (1998) 437–447

PHYSICA D

Frequency analysis of discrete breather modes using a continuous wavelet transform

Kyle Forinash *, W. Christopher Lang

Natural Sciences Division, Indiana University Southeast, New Albany, IN 47150, USA

Abstract

Previous theoretical and numerical studies have shown the conditions for existence and stability properties of intrinsic localized modes (often refered to as discrete breathers) which exist in the gaps outside the linear dispersion bands in anharmonic lattices. We apply a continuous wavelet transform to numerical simulations in order to verify some of the predicted frequency behaviour. Copyright © 1998 Elsevier Science B.V.

1. Introduction

A great deal of the behaviour of intrinsic localized modes (referred to in many papers as discrete breathers) is now well known (see [1] and references therein for a recent review of the current status of discrete breathers). Wavelet transforms have been used for some time now as an inprovement over Fourier transforms in engineering applications where it is desirable to have information about frequencies which change in time. We present here a simple introduction to the continuous wavelet transform and preliminary results showing how the wavelet transform can be used to examine some of the frequency behaviour of intrinsic localized modes.

One property of breathers is that they exist in the gaps outside the linear phonon band. If the breather frequency or a multiple (harmonic) approaches the band, the breather can interact with the phonon band and lose energy. This can result in the total destabilization of the breather or the breather may lose energy in such a way as to move its frequencies away from the phonon band, thus becoming stable. It has also been known for some time that some continuous nonlinear systems experience a modulational instability which leads to self-focusing of energy (the so-called Benjamin–Feir [2] instabilty). Recently, the behaviour of discrete systems experiencing this kind of instability has been examined [3,4]. One key result seems to be the generation of discrete breather modes from band edge phonons as a result of such instability [5].

In Section 2 we give the parameters and equations for the model which was investigated. Section 3 describes the continuous wavelet transform of Grossman and Morlet and indicates how it can be used to monitor single particle

* Corresponding author. E-mail: forinas@indiana.edu.

PII S0167-2789(98)00141-9

frequency changes in the lattice. We indicate some of our results in investigating the behaviour of approximate breather solutions in Section 4. Modulational instability resulting in the formation of a discrete breather is examined in Section 5. In Section 6 we show the results of a spatial transform of the entire chain for two time sliees. A eonclusion is found in Section 7.

2. Model parameters

We consider a simple lattice model which eonsists of a chain of harmonically coupled particles subjected to an asymmetric on-site potential.

The Hamiltonian of the model is

$$H = \sum_n \left[\frac{1}{2}\dot{u}_n^2 + \frac{1}{2}k(u_n - u_{n-1})^2 + V(u_n) \right], \tag{2.1}$$

where the potential is

$$V(u_n) = \omega_0^2 \left(\frac{u_n^2}{2} - \frac{u_n^3}{3} \right). \tag{2.2}$$

In these expressions, the position of particle n is written as a dimensionless variable u_n; time and space have been scaled to have a unit mass for the particles. The parameter ω_0 measures the relative scale of the on-site potential relative to discreteness and of the coupling energy. Large values of ω_0 correspond to the weakly coupled case where the effects of lattice discreteness are large. In this paper all the simulations have been performed with $\omega_0 = 3.2$. This is a moderately discrete case so that the breathers we investigate are localized on a few lattice sites, but are not completely trapped by the pinning potential due to the lattice.

The linear dispersion relation is given by

$$\omega^2 = \omega_0^2 + 4k \sin^2(q/2) \tag{2.3}$$

where q is the linear wave vector and the lattice spacing is taken to be unity. As can be seen from the dispersion relation there is a gap below ω_0 in which there is the potential for stable discrete breathers to exist, provided they do not have a multiple of their frequency lying in the linear phonon band. A chain of 600 particles was chosen for all the simulations and a fifth-order Runga–Kutta method was used which provided energy conservation of better than 0.001%.

3. The continuous wavelet transform

To trace the frequency of a single particle on the chain as it changes over time, we use the continuous wavelet transform of Grossman and Morlet. For a function f on the line, this is defined by

$$Wf(t,\xi) = \int_{-\infty}^{\infty} f(x) w(\xi(x-t))\xi \, dx, \tag{3.1}$$

where $w(x) = (1/\sigma\sqrt{2\pi})e^{i2\pi x}e^{-x^2/2\sigma^2}$. The transform $Wf(t,\xi)$ gives information about the energy content of the signal f at time t and frequency ξ. In this paper we give spectrograms which are plottings of $|Wf(t,\xi)|$ for (typically) $0 \le t \le 72$ s and $2 \le \xi \le 4$ Hz; the wavelet variance σ is typically chosen to be 8 s. (The spectrograms

are rendered as density plottings; the density is always arbitrarily scaled to fit the available range of intensity values. Also the vertical scale is logarithmic, to show equal octaves of frequency equally spaced.)

The underlying idea of the wavelet transform is similar to that of the "windowed" Fourier transform, defined by

$$T_g(t,\xi) = \int_{-\infty}^{\infty} f(x)g(x-t)e^{i2\pi\xi x}\,dx;$$

this is the Fourier transform with a window function g inserted, which limits the calculation of frequency to an interval of time around time t. (The window function g can be chosen to be a Gaussian, which results in a Gabor transform.) The wavelet transform differs from this transform in that the "window" changes width as the frequency ξ is changed: for high frequencies, the window is narrow (which will catch rapid changes in frequency better); for low frequencies, the window is wider (which localizes frequency better, since more cycles of the complex exponential are visible in the integral). Thus the continuous wavelet transform is well-suited for localizing frequency and for localizing time; the windowed Fourier transform can often localize one well but not the other.

Of course, there is a limitation to how well, time and frequency can both be localized; in fact, this is the uncertainty principle, the mathematical form of which states that a function and its Fourier transform cannot both have small support. This limitation manifests itself in our renderings as a trade-off between how "blurry" the image is vertically (i.e., localization of frequency), and how blurry the image is horizontally (i.e., localization of time).

The mathematical statement of the uncertainty principle is that the product of the "width" of a function and the width of its Fourier transform must exceed a certain absolute constant (by width we mean essentially the notion of variance from probability theory). It turns out that product of the widths is the smallest for Gaussian functions; this implies that Gaussian wavelets are well-suited for frequency–time localization.

It should be noted that there are many variations in wavelet construction and application; often discrete wavelet transforms are used instead of continuous transforms. This amounts to computing $W(t,\xi)$ for a discrete set of (t,ξ) (often only ξ equal to powers of two are considered). The advantages of discrete wavelet transforms often include fast algorithms; here we use the continuous transform because we desire complete information about frequency as well as time. For more information about using the continuous wavelet transform for frequency/time analysis, see [6]. A good mathematical reference is [7]. There is a large literature on wavelet analysis; see the Wavelet Digest [1] for bibliographies and other current information about this field.

4. Single particle time transforms

The Hamiltonian (2.1) has large amplitude breather-like solutions which are stabilized by discreteness [8]. They can have an amplitude approaching 1, i.e. approaching the turning point of the potential, and are perfectly stable. No analytical solutions for breathers are known yet, however there are now several numerical methods for arriving at such solutions (see [1] for details and references). In some of the following simulations approximate solutions following from the semi-discrete method were used. We purposely choose an approximate solution over exact solutions because it seems doubtful that in real physical systems a mechanism exists for the generation of exact breathers. Our approximate solutions show an interesting and unexpected behaviour as shown below which demonstrates the utility of the wavelet analysis.

The semi-discrete method uses an expansion of the displacements $u_n(t)$ as

$$u_n(t) = \epsilon[F_{1,n}(t)e^{i\theta_n} + \mathrm{CC}] + \epsilon^2[F_{0,n}(t) + F_{2,n}(t)e^{i2\theta_n} + \mathrm{CC}] + \mathrm{O}(\epsilon^3), \tag{4.1}$$

[1] http://www.wavelet.arg/wavelet/index.html.

with $\theta_n = qn - \omega t$ where q and ω are related by the lattice dispersion relation (2.3). Here CC means complex conjugate. The functions $F_{l,n}$ are assumed to be slowly varying in time and from site to site, and they are determined in the continuum limit. Following the standard reductive perturbation method, and using the new variables $T = \epsilon^2 t$ and $X = \epsilon(x - V_g t)$ with $V_g = \mathrm{d}\omega/\mathrm{d}q$, we obtain the nonlinear Schrödinger (NLS) equation for $F_1(X, T)$

$$\mathrm{i}F_{1,T} + PF_{1,XX} + Q|F_1|^2 F_1 = 0,$$

with

$$Q = \frac{\omega_0^2}{\omega^2}\frac{5\omega_0^2 + 32\sin^4(q/2)}{3\omega_0^2 + 16\sin^4(q/2)}, \qquad P = \frac{\omega_0^2 \cos q - 4\sin^4(q/2)}{2\omega^3}.$$

The breather solution is given by [8]

$$u_n(t) = 2\epsilon A' \mathrm{sech}[\epsilon(n - V_\mathrm{e}t)/L_\mathrm{e}]\cos(\Theta n - \omega_\mathrm{b}t) + 2\epsilon^2 A'^2 \mathrm{sech}^2[\epsilon(n - V_\mathrm{e}t)/L_\mathrm{e}] \times \left\{1 - \frac{1}{3 + (16/\omega_0^2)\sin^4(q/2)}\cos[2(\Theta n - \omega_\mathrm{b}t)]\right\} \tag{4.2}$$

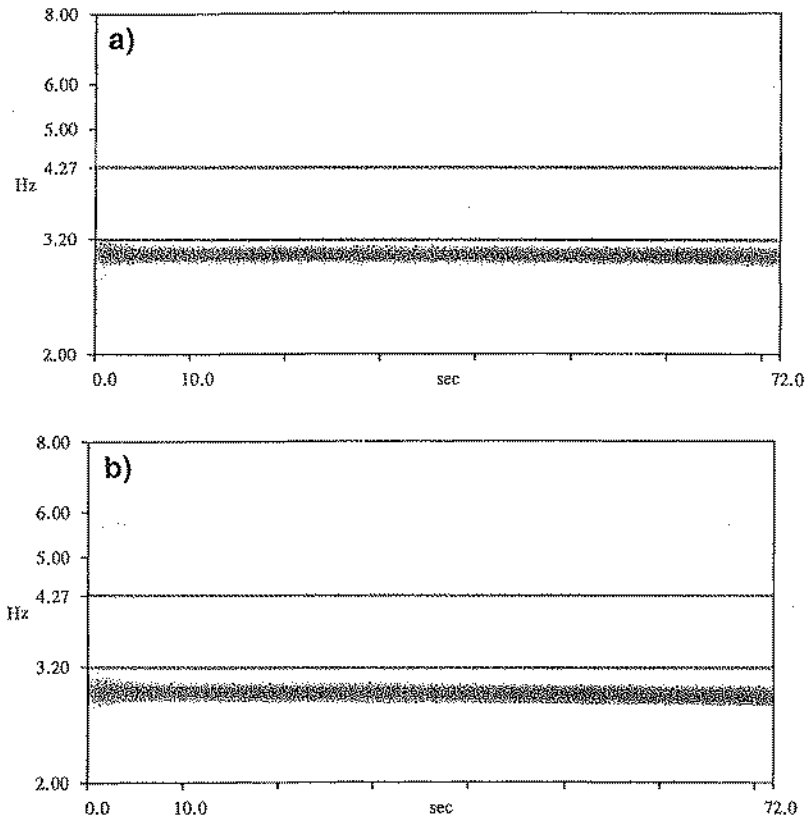

Fig. 1. (a) The wavelet transform of breather of amplitude $A' = 0.30$ and frequency $\omega_\mathrm{b} = 2.96$ Hz. A harmonic can be seen at $2 \times \omega_\mathrm{b} = 5.92$ Hz. Note that the vertical scale is logarithmic. The phonon band is bracketted by grey lines. (b) Increasing the amplitude to $A' = 0.32$ lowers the freqnency to 2.93 Hz and the harmonic above the band shifts towards the linear band.

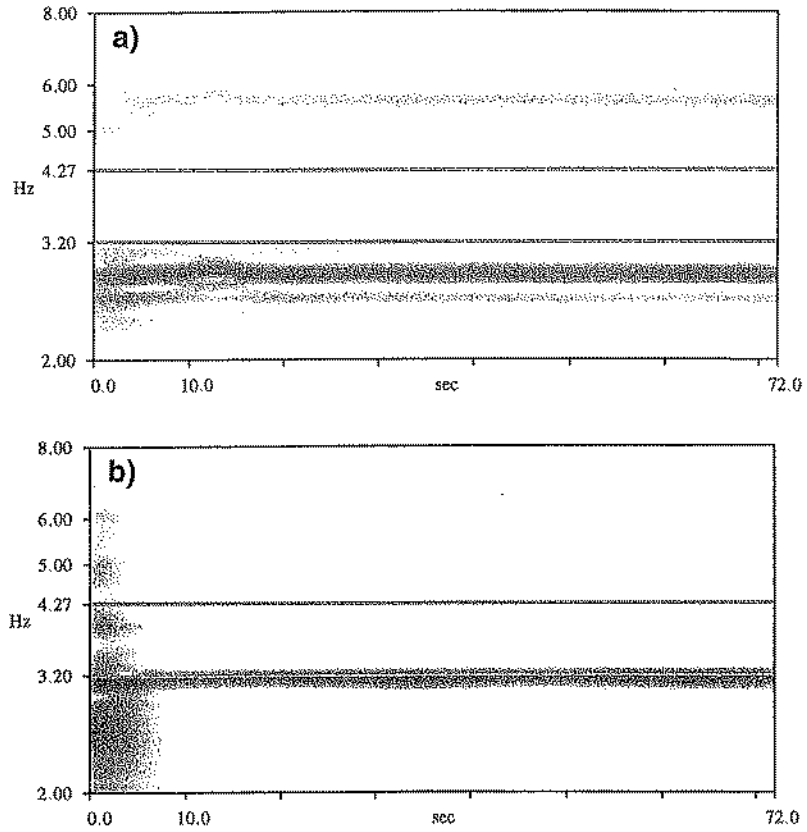

Fig. 2. (a) The frequencies present in a breather of amplitude $A' = 0.34$. Secondary frequencies appear slightly above and below the main breather frequency (at $\omega_b = 2.93$) in addition to the harmonic at $2 \times \omega_b$. (b) The frequencies which result from the collapse of a breather of amplitude $A' = 0.342$. The collapse itself is quite sudden and is not adequately captured by the wavelet transform. Note the very faint frequency bands visible slightly above 6 Hz and in the phonon band.

with

$$A' = \left(\frac{u_e^2 - 2u_e u_c}{2PQ}\right)^{1/2}, \quad L_e = \frac{2P}{(u_e^2 - 2u_e u_c)^{1/2}}$$
$$V_e = V_g + \epsilon u_e, \quad \Theta = q + \epsilon u_e/2P, \tag{4.3}$$
$$\omega_b = \omega + (V_g + \epsilon u_c)\epsilon u_e/2P.$$

The parameters u_e and u_c, which are the velocities of the envelope and carrier waves determine the characteristics of the solution together with the wave vector q chosen for the carrier wave. In our simulations with breather initial conditions we have chosen $q = 0.2$, $u_c = 0$ and the envelope velocity $u_e = 0$; the amplitude A' is an input parameter. Other parameter values are determined from these chosen values. Wavelet transforms were applied to the amplitude of the central site of the breather.

It seems clear from the literature that when the breather frequency ω_b or any multiple reaches the linear band the breather will be able to emit linear phonons and begin to decay. It can be predicted therefore that increasing the amplitude of a breather (which lowers its frequency) in the present model will eventually bring the first harmonic $2 \times \omega_b$ into the band. The lowering of a harmonic of the breather towards the upper band edge can be seen by comparing Figs. 1(a) and (b). In Fig. 1(a) the input amplitude of the breather is $A' = 0.30$, the speed is zero and

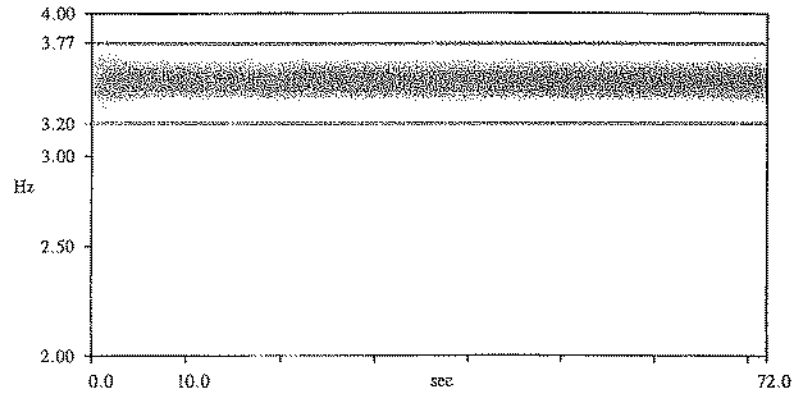

Fig. 3. The transform of an initial sine wave of cycle number $p = 160$ which falls in the region of stability.

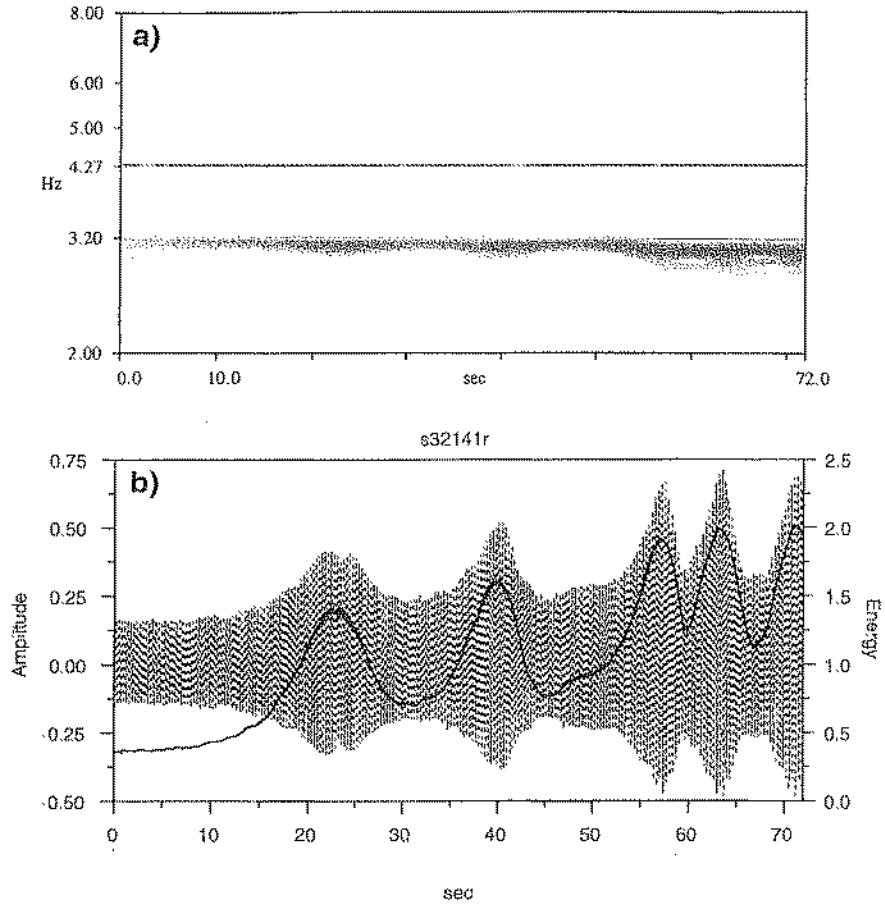

Fig. 4. (a) The wavelet transform of the formation of breather modes from the bottom edge of the linear band for an initial sine wave of $p = 14$ cycles. (b) The related breather amplitude (shaded) and the combined energy of the three sites centred on the breather (dark line) for the same time period.

the harmonic coupling constant $k = 2.0$. This gives a breather frequency of $\omega_b = 2.96$ Hz and a harmonic at 5.92 which clearly is shown in the figure. Increasing the amplitude to $A' = 0.32$ lowers the frequency to 2.93 and Fig. 1(b) shows a harmonic above the band which is lower. One might conclude that continued increase in the breather amplitude will eventually cause a breather frequency with a harmonic at the top of the band and subsequent destabilization of the breather.

However, for the approximate solutions used in these simulations a secondary effect is responsible for the collapse of a larger amplitude breather before the amplitude can be increased to the point that the harmonic of the frequency is at the top of the band. Fig. 2(a) shows the frequencies present in a breather of amplitude $A' = 0.34$. Although the energy and amplitude of this breather is as stable as the $A' = 0.32$ case the presence of secondary frequencies slightly above and below the breather frequency (at $\omega_b = 2.93$) indicate that the initial conditions have relaxed into a different type of breather. Inspection of the stabilty over time of energy and amplitude does not differentiate between these two approximate solutions but a wavelet analysis clearly does.

If the amplitude is increased further to $A' = 0.342$ these side bands of the breather enter the *lower* band edge and cause the breather to give up large amounts of energy. The transition occurs too quickly to be captured entirely by the wavelet analysis but the results of the collapse are clear. As can be seen in Fig. 2(b) a much smaller breather with

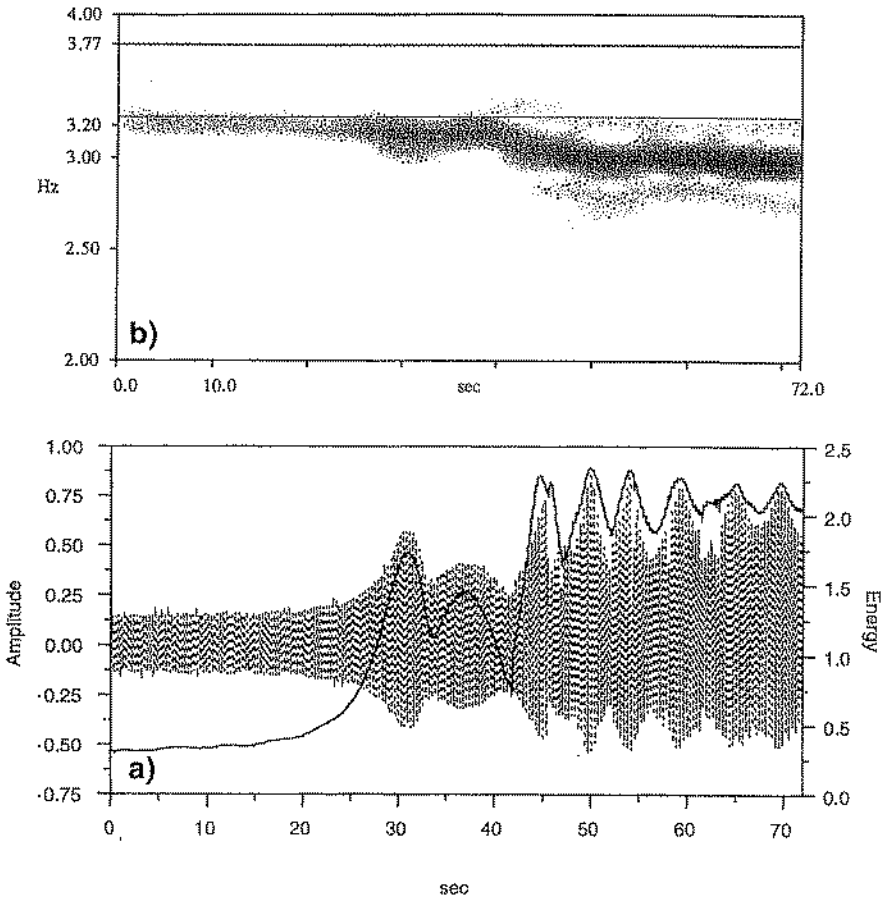

Fig. 5. (a) The wavelet transform of the formation of breather modes from the bottom edge of the linear band for an initial sine wave of $p = 16$ cycles. (b) The related amplitude and the combined energy of the three sites centred on the breather for the same time period. The amplitude is shown by the shaded region and the amplitude is indicated with a dark line.

a frequency just below the band forms. A faint harmonic can be seen just above 6 Hz and an even fainter frequency can be seen near the middle of the band. Evidently low amplitude phonons were created in the linear band from the energy lost by the breather.

5. Modulational instability

In the following the harmonic parameter $k = 1.0$ so that the top of the dispersion band is now at 3.77 Hz. Travelling sine waves of various wavelength corresponding to different locations in the linear dispersion band were used as initial conditions, all with amplitude $A' = 0.14$. Both small sinusoidal modulations (with wavelengths different from the main wave) and small random amplitude perturbations of maximum amplitude 0.01 were used to seed the modulational instability. There was no qualitative difference found between these two types of modulations.

Kivshar et al. [3] have shown by linear stability analysis in the rotating wave approximation that regions of modulational instability exist in the linear band for the model at hand. They show that for $\omega_0^2 \gg 4k$ and amplitude squared smaller than $2k/3$ sine waves are stable for wave vectors $\pi < q < \pi/2$ and unstable for $\pi/2 < q < 0$. Fig. 3 shows the wavelet transform of the case of an initial travelling sine wave with 160 cycles on the chain of 600 sites. The wave vector is given by $q = 2p\pi/N$ where p is the number of wavelengths or cycles on the chain ($p = 150$ cycles corresponds to the cut-off between stable and unstable regimes). As can be seen, this wave falls in the stable band and the oscillations remain there, as does any number of intial cycles greater than $p = 150$.

For $p < 150$ we expect to see modulational instability and subsequent energy localization. Flach [4] and also Sandusky et al. [5] discuss in models different from the present one the formation of discrete breathers from the edge of the phonon band. Figs. 4 and 5 show the formation of breather modes from the bottom edge of the linear band in the present model for an initial sine wave of $p = 14$ and 16 cycles, respectively. In these figures the site of maximum energy was followed and the amplitude of this site was analysed with the wavelet transform. The single site amplitude and energy of that site plus the two neighbouring sites are plotted in the second part of each figure for comparison. Clearly the predicted results of Flach and Sandusky et al. are correct; discrete breathers can form from the band edge (in this case the bottom of the band rather than the top).

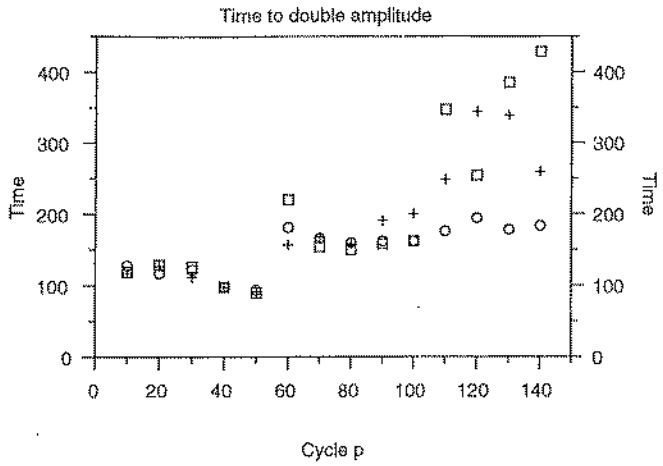

Fig. 6. The length of time until the amplitude is greater than twice the initial amplitude somewhere on the chain for initial sine waves of different wave vectors $q = 2p\pi/N$ where p, the number of cycles on the chain, is an integer. The boxes indicate waves modulated with a sine wave of wavelength 48, the + symbol indicates modulation with a sine wave of wavelength 24 and the circles indicate a random modulation. All modulations were of maximum magnitude 0.01 compared to the initial sine wave condition of amplitude 0.14.

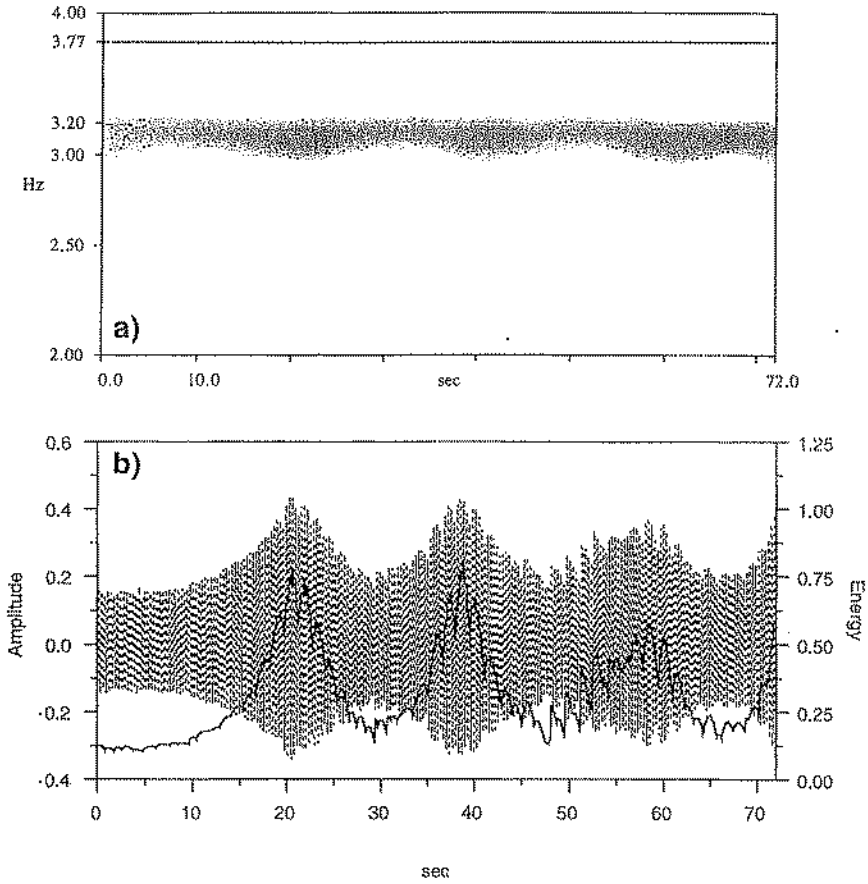

Fig. 7. (a) The wavelet transform of the case of an initial travelling sine wave with 40 cycles on the chain of 600 sites. (b) The amplitude (shaded) of the site and it shows the energy (dark line) of the three sites centred on the maximum energy site. As can be seen from the transform, as the wave attempts to grow in size, additional frequencies appear near the top of the band which prevent further growth.

It is not clear from the analytical analysis that exactly what final outcome should be expected from initial conditions of waves in the instability region which begin far from the band edge. A crude determination of the length of time until the amplitude doubles somewhere on the chain, shown in Fig. 6 for different kinds of modulations, indicates that there may be some undiscovered dynamics for non-band-edge phonons. We were unable to find long lasting breathers arrising from initial conditions $p > 60$; narrow large amplitude oscillations were present but short-lived. The wavelet transform given in Fig. 7 of the case $p = 40$ may indicate that why larger p values give rise to chaotic behavior rather than breathers. As can be seen in the figure a breather does form in this case but as the energy localizes resonance frequencies appear, near the top of the band. When the resonances appear, the amplitude decreases and the frequency of the breather shifts back towards the band edge. These resonances were not seen in the band edge initial conditions and their source is unknown at present.

6. Spatial transform

The continuous wavelet transform can also be used to analyse spatial data as well as time data. Hori [9] has shown that the spatial discrete wavelet transform of a chain with discrete breathers is well suited to describing the spatial

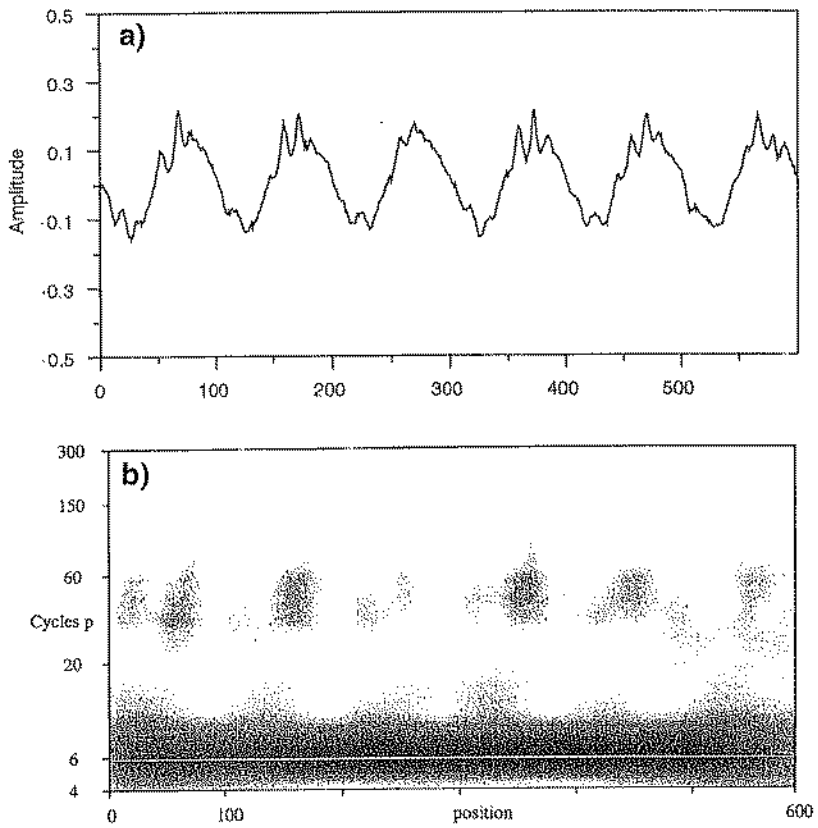

Fig. 8. (a) and (b) show, respectively, the actual amplitude and the spatial wavelet transform of the entire chain of 600 sites at an early time slice for 6 cycles on the chain. (c) and (d) show, respectively, the actual amplitude and the spatial wavelet transform of the entire chain of 600 sites at a later time slice for the same initial conditions. Clearly the 6 Hz signal is disappearing and is being replaced with Dirac delta type spikes which represent the multiple spatial frequencies needed to describe a very narrow discrete breather.

localization of discrete breathers on a lattice. We show a continous wavelet transform of the spatial amplitude of a chain at two different time slices in Fig. 8. A travelling sine wave with small random perturbation was used as an initial configuration. In Figs. 8(a) and (b) an early time slice is shown where the masses are still approximately in their initial mode (a sinusoidal state with six periods down the length of the chain). Fig. 8(a) shows the actual amplitudes and Fig. 8(b) shows the wavelet transform. Figs. 8(c) and (d) shows the actual amplitudes and spatial transform of a later time slice where most of the energy has been localized into a number of breather modes. In the first wavelet transform, note the concentration of energy in the band across the plotting at wave number 6. In the second transform, the energy in that band is much less, while the energy in much higher wave numbers is greater. The tall triangular spike-like objects are typical of highly localized objects (in space) which require many spatial frequencies to describe them accurately.

7. Conclusions

In this paper we have used the wavelet transform to examine the frequencies present in (approximate solution) discrete breathers and the interaction of those frequencies with the linear phonon band. We also followed the

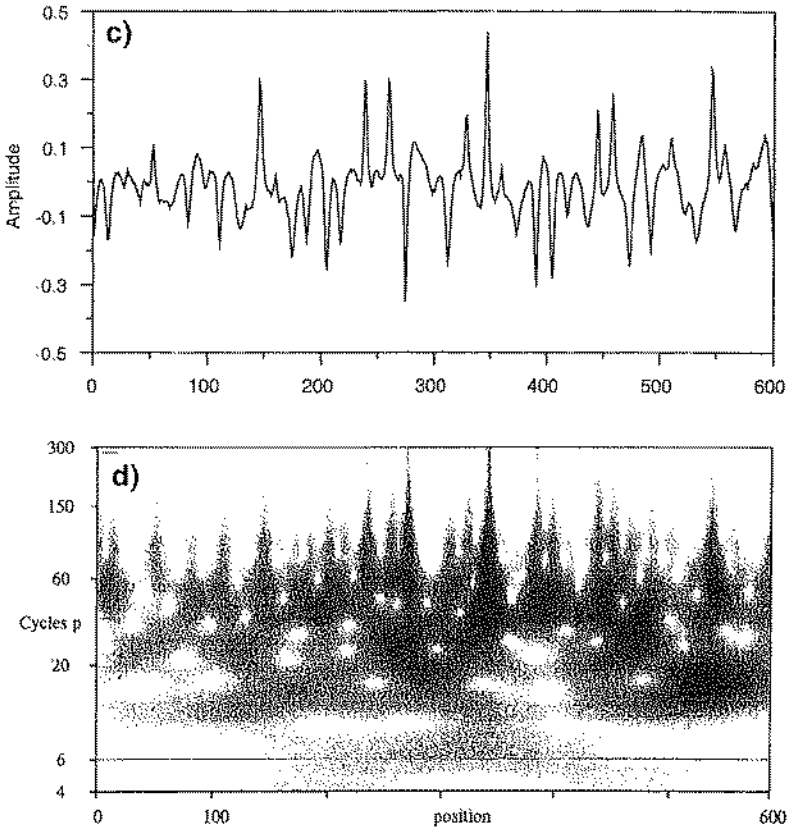

Fig. 8. Continued

time evolution of modulational instability of initial sine waves into discrete breather modes from a single particle frequency perspective. The spatial wavelet transform of the entire chain at different time slices was also examined. We are still at a very preliminary stage of investigation of nonlinear systems using the continuous wavelet transform but we feel examples given in this paper demonstrate the potential of the method for revealing the dynamics of nonlinear behaviour in discrete systems.

References

[1] S. Flach, C.R. Willis, Discrete Breathers, Phys. Rep., to be published 1997.
[2] T.B. Benjamin, J.E. Feir, J. Fluid Mech. A 27 (1967) 417.
[3] Y.S. Kivshar, M. Peyrard, Phys. Rev. A 46 (1992) 3198.
[4] S. Flach, Physica D 91 (1996) 223.
[5] K.W. Sandusky, J.B. Page, Phys. Rev. B 50 (1994) 866.
[6] W.C. Lang, K. Forinash, Time-frequency analysis with the continuous wavelet transform, Am. J. Phys., accepted.
[7] M. Holschneider, Wavelets, An Analysis Tool Clarendon Press, Oxford, 1995.
[8] T. Dauxois, M. Peyrard, C.R. Willis, Physica D 57 (1992) 267.
[9] K. Hori, J. Phys. Soc. Japan 62 (1993) 1819.